

MULTISCALE MASS-SPRING MODELS OF CARBON NANOTUBE ARRAYS ACCOUNTING FOR MULLINS-LIKE BEHAVIOR AND PERMANENT DEFORMATION*

T. BLESSEN[†], F. FRATERNALI[‡], J. R. RANEY[§], AND C. DARAI[§]

Abstract. Based on a one-dimensional discrete system of bistable springs, a mechanical model is introduced to describe plasticity and damage in carbon nanotube (CNT) arrays. The energetics of the mechanical system are investigated analytically, the stress-strain law is derived, and the mechanical dissipation is computed, both for the discrete case as well as for the continuum limit. An information-passing approach is developed that permits the investigation of macroscopic portions of the material. As an application, the simulation of a cyclic compression experiment on real CNT foam is performed, considering both the material response during the primary loading path from the virgin state and the damaged response after preconditioning.

Key words. carbon nanotube arrays, bistable springs, multiscale behavior, Mullins effect, permanent deformation

AMS subject classifications. 74A45, 74D10, 74N30

DOI. 10.1137/12087311X

1. Introduction. Carbon nanotubes (CNTs) have been of great interest for a variety of applications due to their combination of excellent mechanical, electrical, and thermal properties combined with a low density [2]. Nominally aligned arrays of CNTs can be synthesized to form low-density, foam-like materials with dissipative behavior in compression [6]. Structures based on these materials have been shown to dissipate more than two orders of magnitude more energy in compression than typical polymeric foams of comparable density [22].

Arrays of CNTs exhibit a stress-strain hysteresis in compression, which in the past has been related to the behavior of open cell foams [6, 16]. In addition to the hysteretic stress-strain relationship, the mechanical response includes several noteworthy features, the physical basis of which is only understood in part. These include strain localization during compression; strain recovery after compression; a diminishing hysteresis area (i.e., diminishing energy dissipation) and peak stress for the first few compressive cycles; and an abrupt shift in stress-strain behavior to that of the pristine material when a previous value of maximum strain is exceeded.

Strain localization has long been noted during the compression of CNT arrays, with uniaxial compression typically resulting in the imposed strain being entirely

*Received by the editors April 10, 2012; accepted for publication (in revised form) February 21, 2013; published electronically May 22, 2013.

<http://www.siam.org/journals/mms/11-2/87311.html>

[†]Max-Planck-Institute for Mathematics in the Sciences, Inselstraße 22-26, D-04103 Leipzig, Germany (blesgen@mis.mpg.de). This author acknowledges the support of the German Research Community (DFG) through grant BL 512 4/1.

[‡]Department of Civil Engineering, University of Salerno, 84084 Fisciano(SA), Italy (f.fraternali@unisa.it). This author acknowledges financial support from the University of Salerno through the FARB 2012 grant.

[§]Engineering and Applied Science, California Institute of Technology, Pasadena, CA 91125 (raney@caltech.edu, daraio@caltech.edu). The third author gratefully acknowledges the U.S. Department of Defense and the Army Research Office for their support via a National Defense Science & Engineering Graduate (NDSEG) fellowship. The fourth author acknowledges support from the Institute for Collaborative Biotechnologies under contract W911NF-09-D-0001 with the Army Research Office.

accommodated by the formation of buckles at the base of the structure, with *base* being defined as the side that was nearest to the growth substrate during synthesis. This behavior is observed whether the CNTs remain bound to the substrate [33, 18] or are removed from it to create a freestanding structure [6], and is therefore generally thought to be a result of a gradient in physical properties that originate with the growth process. The result of this is that the CNT arrays undergo coordinated buckling of many individual CNTs [37], leading to the formation of buckles, which form sequentially from the base upward [18].

A variety of behaviors has been observed for strain recovery, with some groups reporting that CNT arrays recover most of their original height after large compressive deformation (e.g., [6, 21]), while others have reported an almost complete absence of strain recovery (e.g., [37, 18]). In the past, the former category has consisted of CNTs that were synthesized by a vapor phase catalyst technique by which catalyst is continually deposited during the synthesis process, whereas the latter has consisted of CNTs that were synthesized by a fixed catalyst approach in which CNTs grow from the surface of a catalyst thin film that is deposited prior to the start of synthesis. However, a process was recently reported that allows for either behavior to be obtained for fixed catalyst synthesized CNTs, a fact that the authors attribute to changes in CNT surface roughness [5]. The physical basis for the strain recovery or lack of recovery remains an active area of investigation.

Even for the CNT arrays that are observed to recover well from compression, repeated loading and unloading of the material results in a slight permanent residual strain and also a hysteretic response of decreasing area (and therefore less dissipated energy) and peak stress relative to earlier cycles. Most of this decrease occurs within a few cycles, at which point the material behaves with a steady-state response that is mostly unchanged for any number of later cycles [6, 32, 31]. This initial decrease in energy dissipation for the first several cycles is often referred to as *preconditioning*, and is observed in many rubbery (e.g., [23]) and biological materials (e.g., [25]). We observe that the preconditioning effect in CNT arrays undergoing compression is a local effect, which only occurs up to the maximum compressive strain that is reached. When the maximum strain of all previous cycles is exceeded in a later cycle, immediately the stress-strain response returns to the primary loading path of the pristine material.

These observations in sum are analogous to the Mullins effect in certain rubbers [23] and have been observed in indentation experiments on CNTs in the past [21]. Namely, the Mullins effect is defined to involve a stress-softening behavior that includes three observations (see, for example, [9, 12]): first, the stress measured at a given fixed value of strain will be lower on unloading than it is on loading (defining a hysteresis); second, for repeated loading and unloading to a given maximum strain, a decreasing maximum stress will be observed for the first several cycles until a steady-state hysteresis is eventually reached; and finally, despite this hysteresis of declining area, when a loading path reaches a higher strain than the maximum strain of all previous cycles, an immediate return to the primary loading path is observed (i.e., the stress-strain curve of the pristine material). All three of these elements are present in a wide series of experiments that we performed on different samples and varying architectures of CNT arrays, including single-layer and multilayer structures [30, 31, 22]. For the sake of example, we show in Figure 1 the stress-strain response that we recorded through quasistatic compression tests on a single-layer CNT foam, which was compressed three times to a maximum overall strain of $\epsilon = 0.4$ and then three times to a maximum strain of $\epsilon = 0.8$ (cf. section 3).

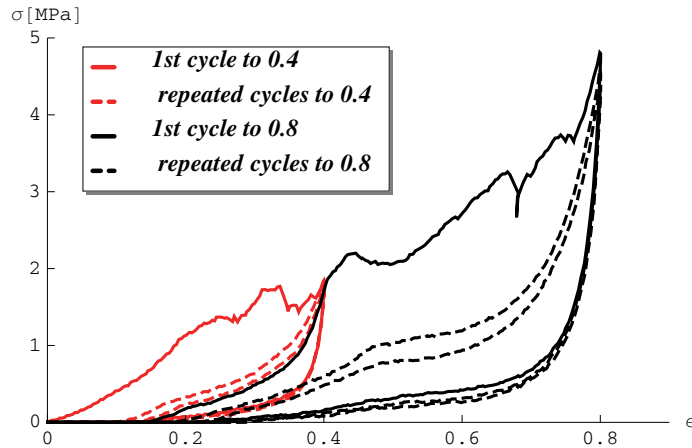


FIG. 1. The stress-strain response of a single-layer CNT sample.

The local rearrangements and buckling associated with preconditioning and the Mullins-like behavior of the CNTs give rise to an important mechanism for energy dissipation during the first few compressive cycles. In some past efforts to model the Mullins effect in reinforced rubber, this source of energy dissipation has been treated as the exclusive source of dissipation (referred to as the *idealized Mullins effect*), with the material behaving elastically after the preconditioning cycles (e.g., [7]). Yet the material continues to exhibit a hysteretic response after preconditioning, as do rubbers, and therefore a model that accounts for both the initial preconditioning cycles (and the Mullins-like strain dependence) as well as the latter hysteretic response of the material is needed. The energy dissipation observed in compressed CNT arrays is a result of the interplay of several distinct mechanisms, including friction and entanglement between CNTs, and possibly viscous flow of air through the interstices [6]. Additionally, individual CNTs have been observed in axial compression to undergo elastic shell buckling, with an unstable kinking regime associated with negative stiffness and resulting dissipation [35, 36]. This latter mechanism leads to a form of rate-independent hysteresis (or “transformational plasticity”) at the macroscopic scale, which is similar to that observed in metals, shape memory alloys, and open-cell foams (refer, e.g., to [28, 24] and references therein).

Bistable spring models in the context of plasticity were introduced in [27]; see also [28] for the investigation of a variety of material behaviors. Typical for such systems is a large number of almost degenerate metastable configurations resulting in a sequence of bifurcations during monotone loading. In magnetism, this kind of mechanism is referred to as the Barkhausen effect [3]. A deeper understanding of how the different length scales interact physically was obtained by the investigation of the pinning and depinning patterns of inhomogeneous materials like superconductors, the occurrence of Bloch walls in ferromagnets, or the formation of crack lines [11].

The approach of bistable springs is in particular appealing for systems undergoing cyclic loading with hysteresis; see, e.g., the recent articles [17] and [26], among others. In [8], bistable springs have also been applied to plastically deformed spider silks. But unlike the model presented here, the stress-strain law is linked to the microstructure. A homogenization of the discrete model is found in [13].

Multiscale mass-spring models of CNT structures have been recently proposed in [14, 30], in order to account for the hysteretic response of single-layer and multilayer structures within an effective one-dimensional framework. Such models are able to capture some distinctive features of the microstructural rearrangements that have been discussed so far, and namely

- strain localization due to local buckling of the tubes;
- rate-independent hysteresis induced by the succession of infinitesimal, negative-stiffness events of viscous nature at the microscopic scale (refer also to [28]);
- multiscale response related to graded mechanical properties along the height of the structure (e.g., [29, 30]).

We show in the present work that a suitable generalization of the above models leads us to capture some other relevant phenomena, such as

- material damage induced by Mullins-like response to preconditioning;
- permanent deformation of the structure.

We start by describing the primary loading path of a CNT array under uniform compression through the multiscale mass-spring model presented in [14]. Subsequently, we introduce some preconditioning-induced material damage by setting to zero the stiffness of a suitable percentage of microscopic springs. Such a position also allows us to model permanent axial deformation of the structure. The latter follows from the irreversible “annihilation” of the springs with zero stiffness and coincides with the “activation” strain of the mesoscopic response. As in [14], we introduce an intermediate mesoscopic scale in between the microscopic scale of an infinitesimal vertical portion of the structure and the scale of the entire structure. This allows us to account for grading of material damage along the thickness of the structure. The mesoscopic response is obtained through an analytic approach, by computing the limiting response of the bistable spring model adopted at the microscopic scale.

An analytic approach to damage in CNT arrays is already given in [4], where the passage from microscale to mesoscale is studied both numerically and analytically in the framework of Γ -convergence for the elastic energy functional. We extend this analysis here by studying the branching mechanism during the minimization process and by computing the dissipated energy, also for the continuum limit of infinitely many springs.

We use an information-passing technique in section 2.3 to formulate a mechanical model of the macroscopic response of the structure. We address to future work the modeling of the transient response of CNT arrays during preconditioning, which might be rate-dependent and account for progressive deterioration of the mechanical properties at the microscopic level.

The paper is organized as follows. First we summarize an earlier model by the authors where bistable mass-spring models have been used to describe the plastic behavior of CNT arrays. In section 2.2, we extend this model to incorporate damage, i.e., the mechanical failure of certain springs. Therein we also study the energy landscape, derive the stress-strain law, and compute the dissipated energy, both for the discrete system as well as for the idealized continuum limit of infinitely many springs. In section 2.3, we develop an information-passing approach to deal with macroscopic sections of a CNT material. These concepts are then combined in section 3 to do simulations for experimental data on multicycle compression tests with very good agreement. We end with an evaluation of the results and an outlook for the future.

2. Multiscale mass-spring models of CNT arrays.

2.1. Bistable spring model at the microscopic scale. We model an infinitesimal portion of a CNT foam through the bistable spring model extensively described in [14], which we hereafter briefly summarize. We assume that such a portion of the foam can be described as a chain of $N + 1$ lumped masses m^0, \dots, m^N , with m^N clamped at the bottom of the chain. The adjacent masses are connected with each other through bistable springs characterized by the following axial strains:

$$(2.1) \quad \varepsilon^i = \varepsilon^i(u_N) = \frac{u_N^{i-1} - u_N^i}{h_N}, \quad i = 1, \dots, N,$$

where $h_N := L/N$ is the equal spacing between the masses, u_N^i denotes the axial displacement of the mass m^i (positive upward), and we set $u_N := \{u_N^0, \dots, u_N^N\}$. The potential V^i and stress σ^i versus strain ε^i laws of the generic spring are defined by

$$(2.2) \quad V^i(\varepsilon^i) = \begin{cases} V_a^i(\varepsilon^i) := -k_0^i[\varepsilon^i + \ln(1 - \varepsilon^i)], & \varepsilon^i < \varepsilon_a^i, \\ V_b^i(\varepsilon^i) := c_1 + \sigma_a^i \varepsilon^i + \frac{1}{2}k_b^i(\varepsilon^i - \varepsilon_a^i)^2, & \varepsilon_a^i \leq \varepsilon^i \leq \bar{\varepsilon}_c^i, \\ V_c^i(\varepsilon^i) := c_2 - k_c^i[\varepsilon^i - \varepsilon_*^i + \ln(1 - (\varepsilon^i - \varepsilon_*^i))], & \bar{\varepsilon}_c^i < \varepsilon^i, \end{cases}$$

$$(2.3) \quad \sigma^i(\varepsilon^i) = V^{i'}(\varepsilon^i) = \begin{cases} k_0^i \frac{\varepsilon^i}{1-\varepsilon^i}, & \varepsilon^i < \varepsilon_a^i, \\ \sigma_a^i + k_b^i(\varepsilon^i - \varepsilon_a^i), & \varepsilon_a^i \leq \varepsilon^i \leq \bar{\varepsilon}_c^i, \\ \frac{k_c^i(\varepsilon^i - \varepsilon_*^i)}{1 - (\varepsilon^i - \varepsilon_*^i)}, & \bar{\varepsilon}_c^i < \varepsilon^i, \end{cases}$$

where $k_0^i > 0$, $k_b^i < 0$, $k_c^i > 0$, $\varepsilon_a^i > 0$, and $\varepsilon_c^i \geq \varepsilon_a^i$ are constitutive parameters (five independent parameters); the constants $c_1 < 0$ and $c_2 > 0$ are such that $V_a^i(\varepsilon_a^i) = V_b^i(\varepsilon_a^i)$, $V_b^i(\bar{\varepsilon}_c^i) = V_c^i(\bar{\varepsilon}_c^i)$. From the continuity of the stress it follows that

$$(2.4) \quad \varepsilon_*^i = \varepsilon_c^i - \frac{\sigma_a^i}{k_c^i + \sigma_a^i},$$

$$(2.5) \quad \bar{\varepsilon}_c^i = \frac{\varepsilon_c^i(k_c^i + \sigma_a^i)}{k_c^i + \sigma_c^i} + \frac{(\sigma_c^i - \sigma_a^i)(k_c^i + \varepsilon_c^i k_c^i + \varepsilon_c^i \sigma_a^i)}{(k_c^i + \sigma_a^i)(k_c^i + \sigma_c^i)},$$

with

$$(2.6) \quad \sigma_a^i = k_0^i \frac{\varepsilon_a^i}{1 - \varepsilon_a^i}, \quad \sigma_c^i = \sigma_a^i + k_b^i(\bar{\varepsilon}_c^i - \varepsilon_a^i).$$

The stress-strain response (2.3) is graphically illustrated in Figure 2.

The introduction of bistable spring elements in situations where there is an unstable transition between the phases (a) and (c) enable us to capture the stress drops observed in the experimental response of CNT foams and pillars which take place in correspondence with the buckling snaps of the tubes; see, e.g., scanning electron microscopy (SEM)-assisted tests [18]. The bistable spring elements allow us to describe the local buckling of the tubes similar to a phase transition from the unbuckled phase to the densification phase.

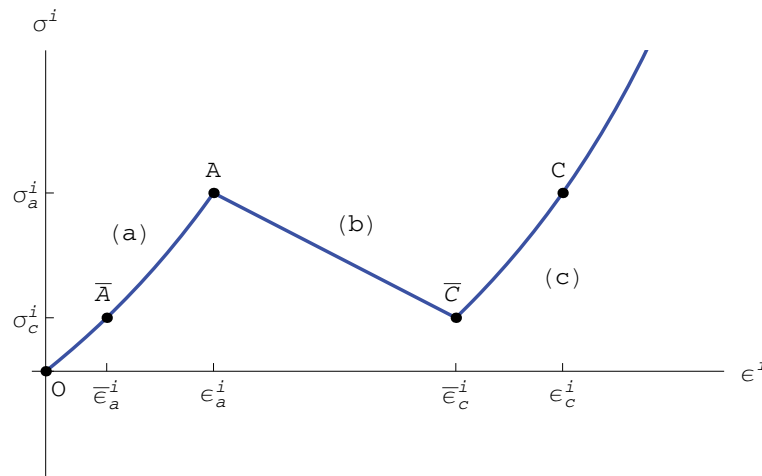


FIG. 2. Stress σ^i versus strain ε^i relationship in the generic microscopic spring.

2.2. Response at the mesoscopic scale. In the present section we study a dynamic switching process at the microscopic scale between the phases (a) and (c) described by branches $O\bar{A}A$ and $\bar{C}C$ in Figure 2, respectively. This is in line with the ideas in [27, 28]. Following [28], we name a response of the material *plastic*, if the strain ε^i of a single spring exceeds the critical value ε_a^i . For a chain of N springs, this can be characterized by the occurrence of loading and unloading stress plateaux. However, we notice that our analysis excludes accumulation of permanent deformation; therefore the end point of one hysteresis cycle coincides with the start point of the next cycle. In this sense, the present hysteresis model is time-independent.

Within the current section, we rescale for simplicity L to unity; name (b) the unstable phase described by branch $\bar{A}\bar{C}$ in Figure 2; and regard a mesoscopic element of a CNT array as the limit for $N \rightarrow \infty$ of a series of N microscopic springs.

Let us refer to the steady-state dissipation following preconditioning as the “hysteretic shakedown” of the material. We assume that the application of a given number m of hysteretic shakedowns (up to different maximum strains) has severely weakened the stiffness of $(1 - \beta(m))N$ microscopic springs for a given number $0 < \beta(m) \leq 1$, and that at the current time for all $m \in \mathbb{N}$ it holds that

- (A1) $k_c^i = k_0^i$ for all $i \in \mathbb{N}$,
- (A2) $k_0^1 = k_0^2 = \dots = k_0^{\lfloor \beta N \rfloor} = k_0$, $k_0^{\lfloor \beta N \rfloor + 1} = \dots = k_0^N = \delta$,
- (A3) $\varepsilon_i^* = \varepsilon_*$ for $1 \leq i \leq \lfloor \beta N \rfloor$,
- (A4) $\varepsilon_a^i = \bar{\varepsilon}_c^i$ for $\lfloor \beta N \rfloor + 1 \leq i \leq N$.

Condition (A1) stipulates the *symmetry* of the microscopic springs. By (A2), we may differentiate between the springs $1, \dots, \lfloor \beta N \rfloor$, which we call from now on *undamaged*, and the remaining springs $\lfloor \beta N \rfloor + 1, \dots, N$, subsequently called *damaged*. The constant k_0 in (A2) is positive. The parameter δ is a small, positive constant and it will become clear later why this parameter has been introduced.

While β captures the phenomenological “damage” associated with changes in the stress-strain response (i.e., a decline in stress levels after the first compressive cycle, residual strain, etc., as discussed earlier), it is important to note that these changing features of the stress-strain response are a result of complex microstructural changes

and not literal damage to the individual CNTs. SEM and transmission electron microscopy (TEM) have shown no damage to the individual CNTs after quasistatic compression of the sort we have performed on our systems, a result of the extreme bendability known to exist in CNTs [10]. Rather, the phenomenological “damage” that is observed at a structural level is a result of a reordering of the CNTs, which is necessary for the formation of collective buckles under compression [37]. Though the CNT arrays continue to recover much of their height in subsequent cycles, and therefore in an important sense the formation of buckles is reversible, the reorientation of the CNTs that is necessary for the formation of these collective buckles is permanent [37, 6]. It is this latter effect that is being captured by β in our model. The twisting and sliding of the individual CNTs relative to one another that occurs during this permanent reordering results in higher observed stress and energy dissipation during earlier compressive cycles (e.g., when the material is entirely “undamaged” with $\beta = 1$) relative to later cycles. The higher energy dissipation during the first cycle could be explained by an increased frequency of the formation and breaking of van der Waals interactions as a result of this twisting and sliding during reorientation of the CNTs, similar to what was recently studied in [34].

The above model with the assumptions (A1)–(A4) has already been introduced in [4], where also the Γ -limit of the energy has been computed. In this article, we are going to extend the analysis and investigate the branch-switching during the minimizing of the total mechanical energy, and in particular compute the dissipation of an array with N masses and perform the dissipation limit when $N \rightarrow \infty$.

For the later analysis we also require a certain smallness condition on ε_a^i and $\bar{\varepsilon}_c^i$ relating to strong pinning that disappears in the limit $N \rightarrow \infty$ [27].

We define the mechanical energy of the structure as

$$(2.7) \quad E_N(u_N) = \frac{1}{N} \sum_{i=1}^N V^i(\varepsilon^i(u_N))$$

with the effective potentials V^i given by (2.2).

Let σ be the given total stress. The mesoscopic average strain is simply

$$\varepsilon(u_N) := \frac{1}{N} \sum_{i=1}^N \varepsilon^i(u_N),$$

where ε^i is the strain associated with the i th spring.

We model plasticity by the gradient flow equations [28]

$$(2.8) \quad \nu \dot{\varepsilon}^i(u_N) = -\frac{\partial \Phi_N}{\partial \varepsilon^i}(\varepsilon^1(u_N), \dots, \varepsilon^N(u_N))$$

with the total energy

$$\Phi_N(\varepsilon^1, \dots, \varepsilon^N) := \frac{1}{N} \sum_{i=1}^N [V^i(\varepsilon^i) - \sigma \varepsilon^i].$$

The evolution equation (2.8) lets ε^i evolve towards local minimizers of Φ_N . We are interested in the limit $\nu \rightarrow 0$ which amounts to infinitely fast evolution such that $\varepsilon(u_N)$ attains a local minimizer of Φ_N . First we construct the equilibrium points.

Inside the i th spring element, the strain must satisfy the condition $(V^i)'(\varepsilon^i) = \sigma$. For given total stress σ , there are at most the three local minimizers (using (A3))

$$(2.9a) \quad \check{\varepsilon}_a^i(m) = \frac{\sigma}{k_0^i + \sigma},$$

$$(2.9b) \quad \check{\varepsilon}_b^i(m) = \frac{\sigma - \sigma_a}{k_b^i} + \varepsilon_a^i,$$

$$(2.9c) \quad \check{\varepsilon}_c^i(m) = \frac{\sigma(1 + \varepsilon_*) + k_0^i \varepsilon_*}{k_0^i + \sigma} = \check{\varepsilon}_a^i(m) + \varepsilon_*.$$

For the derivation of (2.9), it is necessary that δ be positive. In (2.9), the values of k_0^i depend on β and hence in turn on m .

In a loading or unloading experiment, the first spring located closer to the bottom of the structure is the softest and yields first, changing its phase [30, 15]. Next, the second spring yields, and so forth, until the $\lfloor \beta N \rfloor$ th spring. (Note that in accordance with (A2) and (A4), the springs $\lfloor \beta N \rfloor + 1, \dots, N$ with spring constant δ do not change their state.) Therefore, similar to the case of N identical springs, the total state of the series of springs is still completely specified by two scalar parameters p and q and the additional parameter β . Here, p , q , $1 - p - q$ denote the phase fractions of the minimizers a , b , and c , which corresponds to having $\beta N p$, $\beta N q$ and $\beta N(1 - p - q)$ springs in phase (a), (b), and (c), respectively. We assumed here that $\beta N p \in \mathbb{N}$.

As $\varepsilon \mapsto V^i(\varepsilon)$ is concave in regime b for all $i \in \mathbb{N}$, if the elongation of a spring in the local minimum $\check{\varepsilon}_b^i$ is altered by an arbitrarily small perturbation, it will move (according to the sign of the perturbation) to either $\check{\varepsilon}_a^i$ or $\check{\varepsilon}_c^i$. In consequence, any system of N springs with $q \neq 0$ is unstable and we may in the following calculations restrict to the case $q = 0$.

The average strain of a system with βN springs in equilibrium and the first $\beta N p$ springs in phase (a) fulfills the identity

$$\begin{aligned} \varepsilon(m) &= \frac{1}{N} \left[\sum_{i=1}^{\beta N p} \check{\varepsilon}_a^i(m) + \sum_{i=\beta N p+1}^{\lfloor \beta N \rfloor} \check{\varepsilon}_c^i(m) + \sum_{i=\lfloor \beta N \rfloor+1}^N \frac{\sigma}{k_0^i + \sigma} \right] \\ &= \frac{1}{N} \sum_{i=1}^{\lfloor \beta N \rfloor} \check{\varepsilon}_a^i(m) + \frac{1}{N} \sum_{i=\beta N p+1}^{\lfloor \beta N \rfloor} \varepsilon_* + \frac{1}{N} \sum_{i=\lfloor \beta N \rfloor+1}^N \frac{\sigma}{\delta + \sigma}. \end{aligned}$$

Since (2.9) is defined for every $\delta > 0$, it is valid to consider the limiting case $\delta \searrow 0$, where the artificial parameter δ disappears. In this case, we obtain

$$(2.10) \quad \begin{aligned} \varepsilon(m) &= \frac{\beta \sigma(m)}{k_0 + \sigma(m)} + (1 - \beta) + \beta(1 - p)\varepsilon_* \\ &= \frac{\sigma(m) + (1 - \beta)k_0}{k_0 + \sigma(m)} + \beta(1 - p)\varepsilon_*, \end{aligned}$$

where we used (A1)–(A4), (2.3) and (2.9). In particular, $\check{\varepsilon}_c^i = \check{\varepsilon}_a^i + \varepsilon_*$ was used. Additionally, when deriving (2.10), we implicitly assumed that $\lim_{\delta \searrow 0} (\delta/\sigma) = 0$.

Resolving (2.10), we obtain the stress-strain relationship for a system with N springs:

$$(2.11) \quad \sigma(\varepsilon, m) = \frac{k_0(\varepsilon - \varepsilon_p + \beta - 1)}{1 - (\varepsilon - \varepsilon_p)}$$

with

$$\varepsilon_p(m) := \beta(1 - p)\varepsilon_*$$

This quantity can in a natural way be identified with the plastic strain. From (2.11) we see that σ only depends on m and on the elastic strain $\varepsilon_{el} := \varepsilon - \varepsilon_p$.

For the energy of the equilibrium configuration with the first Np springs in phase (a), we find

$$\begin{aligned} \widehat{E}_p(\varepsilon, m) &= \frac{1}{N} \left[\sum_{i=1}^{\beta Np} V^i(\varepsilon_a^i(m)) + \sum_{i=\beta Np+1}^{[\beta N]} V^i(\varepsilon_c^i(m)) \right] \\ &= \frac{1}{N} \sum_{i=1}^{[\beta N]} (-k_0^i) \left[\frac{\sigma(\varepsilon, m)}{k_0^i + \sigma(\varepsilon, m)} + \ln \left(\frac{k_0^i}{k_0^i + \sigma(\varepsilon, m)} \right) \right] + (1-p)c_2. \end{aligned}$$

Since

$$\frac{\sigma(\varepsilon, m)}{k_0 + \sigma(\varepsilon, m)} = \frac{\varepsilon - \varepsilon_p(m) + \beta - 1}{\beta}, \quad \frac{k_0}{k_0 + \sigma(\varepsilon, m)} = \frac{1 - (\varepsilon - \varepsilon_p(m))}{\beta},$$

we end up with

$$\widehat{E}_p(\varepsilon, m) = (-k_0) \left[\varepsilon - \varepsilon_p(m) + \beta - 1 + \beta \ln \left(\frac{1 - (\varepsilon - \varepsilon_p(m))}{\beta} \right) \right] + \beta(1-p)c_2.$$

By straightforward computations, we find for the derivative

$$\frac{\partial \widehat{E}_p(\varepsilon, m)}{\partial \varepsilon} = (k_0) \frac{\varepsilon - \varepsilon_p(m) + \beta - 1}{1 - (\varepsilon - \varepsilon_p(m))}.$$

For fixed m , the functionals \widehat{E}_p constitute a family of convex functionals with a finite number of local minimizers (depending on the parameter p). The switching takes place between branches that differ in exactly one element in phase space and the succession of N such steps describes the transition from one homogeneous state to the next. Each of these steps can be thought of as the combination of an elastic part and a plastic part.

The stress-strain curve of the structure follows a sawtooth pattern as illustrated in Figure 3. The symbols P^i denote the final states of the *elastic steps* ($Q^i \rightarrow P^{i+1}$) where the system remains on the same metastable branch as long as possible. The *plastic steps* ($P^i \rightarrow Q^i$) are characterized by the fact that the total strain is fixed and the system switches between metastable branches that are neighbors ($[Np] = 1$, and $[(\cdot)]$ generically denotes the jump of a quantity (\cdot)). It is worth observing that stress is zero for $\varepsilon \leq 1 - \beta$, and that, conversely, the system is able to bear stresses $\sigma > 0$ for $\varepsilon > 1 - \beta$, even in presence of $(1 - \beta)N$ springs with stiffness k_0^i tending to zero. This is possible because the local strain ε^i in such springs remains constantly equal to unity.

For the next step of the analysis, in addition to (A1)–(A4), we assume

$$(2.12) \quad (A5) \quad \varepsilon_a^i \equiv \varepsilon_a, \quad \varepsilon_c^i \equiv \varepsilon_c \quad \text{for all } i \in \mathbb{N}.$$

The above considerations then lead for $1 \leq i \leq N$ to the representation

$$P^i = \left(\varepsilon_{P_i}, \frac{k_0(\varepsilon_a + \beta - 1)}{1 - \varepsilon_a} \right), \quad Q^i = \left(\varepsilon_{P_i}, \frac{k_0(\varepsilon_a - \beta\varepsilon_*/N + \beta - 1)}{1 - \varepsilon_a + \beta\varepsilon_*/N} \right)$$

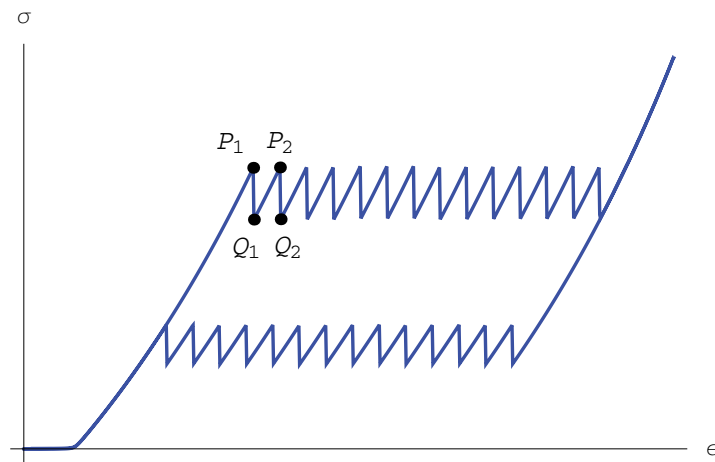


FIG. 3. Overall stress-strain pattern of a finite series of microscopic springs.

in the (ε, σ) -diagram, where

$$(2.13) \quad \varepsilon_{P_i} := \varepsilon_a + \frac{i-1}{N} \beta \varepsilon_*.$$

So we can compute that a plastic step is characterized by

$$[\varepsilon] = 0, \quad [Np] = 1, \quad [\sigma] = -(\beta^2 k_0) \frac{\varepsilon_*}{N(1-\varepsilon_a)(1-\varepsilon_a + \beta \varepsilon_*/N)},$$

whereas an elastic step fulfills

$$[\varepsilon] = \beta \frac{\varepsilon_*}{N}, \quad [Np] = 0, \quad [\sigma] = (\beta^2 k_0) \frac{\varepsilon_*}{N(1-\varepsilon_a)(1-\varepsilon_a + \beta \varepsilon_*/N)}.$$

The evolution equation (2.8) lets ε^i evolve towards local minimizers of Φ_N .

Now we want to look at the energetics of the plastic and the elastic regime. For an elastic step we have the energy difference

$$(2.14) \quad \Delta \hat{E}_N = \beta k_0 \left[\ln(1 - \varepsilon_a + \beta \varepsilon_*(1 - N)/N) - \ln(1 - \varepsilon_a + \beta \varepsilon_*(2 - N)/N) \right] + \frac{k_0 \beta}{N} \varepsilon_*.$$

In the same spirit, we calculate that for a system with $N \geq 1$ springs, the plastic dissipation is

$$(2.15) \quad \begin{aligned} D_N &= \beta k_0 \left[\ln(1 - \varepsilon_a + \beta \varepsilon_*(2 - N)/N) - \ln(1 - \varepsilon_a + \beta \varepsilon_*(1 - N)/N) \right] - \frac{\beta(c_2 + k_0 \varepsilon_*)}{N} \\ &= \beta k_0 \frac{1}{\xi_N} \frac{\beta \varepsilon_*}{N} - \frac{\beta(c_2 + k_0 \varepsilon_*)}{N} \end{aligned}$$

for a parameter

$$\xi_N \in \left(1 - \varepsilon_a + \frac{1-N}{N} \beta \varepsilon_*, 1 - \varepsilon_a + \frac{2-N}{N} \beta \varepsilon_* \right).$$

Clearly, $\xi_N \rightarrow 1 - \varepsilon_a - \beta\varepsilon_*$ for $N \rightarrow \infty$.

In one hysteresis cycle, there are $\lfloor \beta N \rfloor$ steps where the stress is increased and $\lfloor \beta N \rfloor$ steps where the material yields and energy is dissipated. Thus, the total dissipated energy D in a cycle becomes in the limit $N \rightarrow \infty$

$$(2.16) \quad D = \lim_{N \rightarrow \infty} (\beta N D_N) = \beta^2 \left(\frac{\beta k_0 \varepsilon_*}{1 - \varepsilon_a - \beta \varepsilon_*} - c_2 - k_0 \varepsilon_* \right).$$

The limit stress-strain pattern for $N \rightarrow \infty$ is shown in Figure 4 for different values of the parameter β . It corresponds to a “perfectly plastic” behavior with stress plateaux at $\sigma = \sigma_a$ (loading plateau) and $\sigma = \sigma_c = \sigma_a + \Delta\sigma$ (unloading plateau). We emphasize again that this ansatz only works for rate-independent plasticity where the energy only depends on the start point and end point of the evolution, but not on the evolution path itself. The limit dissipation (2.16) equals the area enclosed by the limit stress-strain response. As already observed, the behavior shown in Figure 4 refers to a mesoscopic spring element, which represents a finite portion of the array thickness. It is worth observing that equation (2.11) is still valid in the limit $N \rightarrow \infty$, with $\varepsilon_p = \beta\varepsilon_*$. This implies that the stress is zero for $\varepsilon \leq 1 - \beta$ in the limiting behavior. We can therefore refer to the quantity $1 - \beta$ as the “activation strain” of the mesoscopic response (or “damage” parameter). Conversely, the quantity β can be regarded as an “integrity” parameter of the material at the mesoscopic scale.

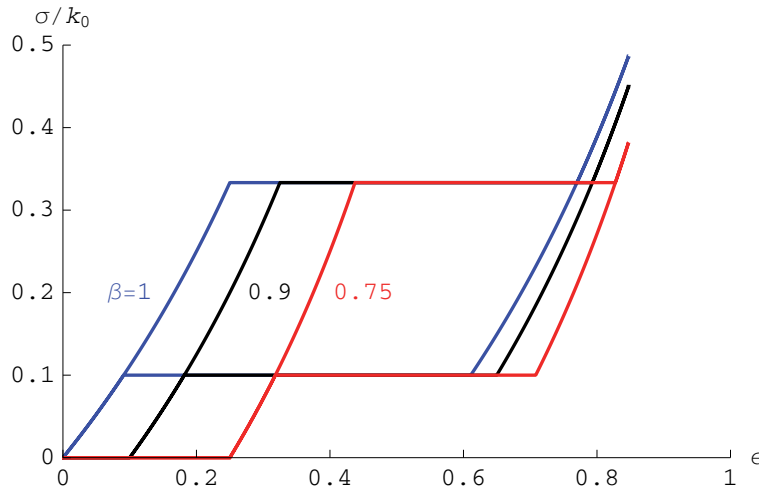


FIG. 4. Overall limiting stress-strain pattern ($N \rightarrow \infty$) as predicted by the Γ -limit for different values of β (fixed material constants: $k_0 = k_c = 50.00 \times 10^6$ Pa; $k_b = -22.44 \times 10^6$ Pa; $\varepsilon_a = 0.25$; $\varepsilon_* = 0.52$; $\delta = 50.00 \times 10^2$ Pa).

2.3. Macroscopic response. We model the macroscopic mechanical response of a CNT array through an information-passing approach (see [14] for an introduction of the method) adopting a mass-spring chain composed of a finite number of mesoscopic springs, and a suitable modification of the analytical model derived in the previous section for each spring.

We already noted that the assumption (A1) introduced in section 2.2 implies that the phases (a) and (b) of the microscopic response (Figure 2) are “symmetric,” while

Assumptions (A2)–(A3) imply that the microscopic springs have uniform mechanical properties.

It is known, however, that real CNT foams exhibit a gradient in density along the height of the tubes, which typically increases from the base to the top (e.g., [29, 18]); and Mullins-like behavior characterized by different stiffness during loading and unloading [21]. In particular, the density gradient typically induces bottom-to-top increasing local buckling loads and progressive tube collapse starting from the bottom [6, 18]. We show in Figure 5 the overall stress-strain response that we numerically determined for chains showing 9 undamaged and 1 damaged springs, and, alternatively, constant material properties (“p.plastic” response), or linearly increasing buckling loads along the thickness (“hardening” response). It is seen that the “hardening” response actually features a sawtooth stress-strain diagram characterized by a progressive increase of the stress σ during the plastic steps, while the “p.plastic” response features a sawtooth stress-strain diagram showing constant average stress (cf. the previous section about the second behavior).

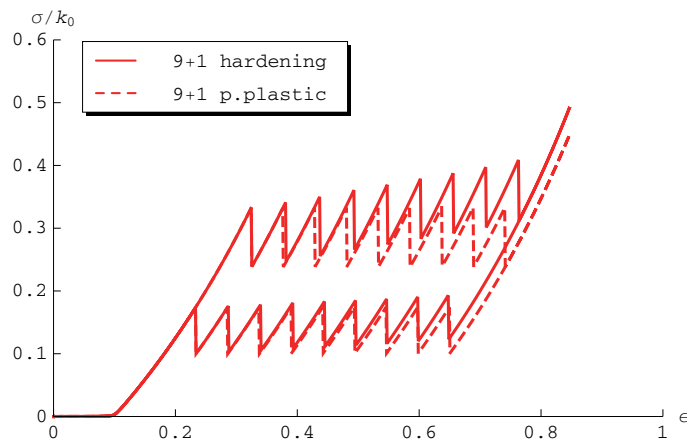


FIG. 5. Overall stress-strain pattern of chains showing 9 undamaged and 1 damaged springs ($\beta = 0.9$). The “p.plastic” response refers to constant ε_a (i.e., constant buckling load; cf. Figure 2) in each spring, while the “hardening” response refers to ε_a linearly varying along the thickness of the chain. Chosen spring constants: $k_0 = k_c = 50.00 \times 10^6$ Pa; $k_b = -22.44 \times 10^6$ Pa; $\varepsilon_a = \text{const} = 0.25$ in the “p.plastic” chain; ε_a varying from 0.25 to 0.29 (step 0.05) in the “hardening” chain; $\varepsilon_* = 0.52$; $\delta = 50.00 \times 10^2$ Pa.

In order to account for graded material properties and different stiffness during loading and unloading, we slightly modify the limiting mesoscopic behavior illustrated in Figure 4, describing the generic mesoscopic spring (say, the i th one) through the following constitutive equation (Figure 6):

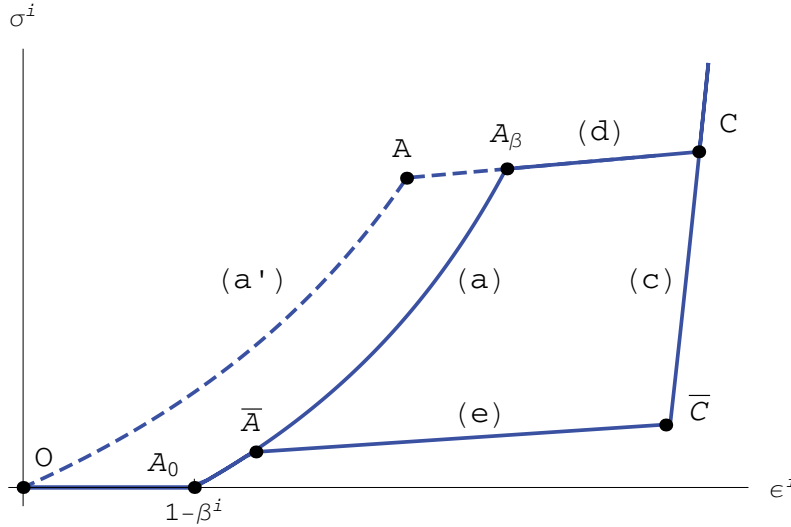


FIG. 6. Modified mesoscopic model account for material hardening during the “plastic” phase transitions (d) and (e), and different rigidities of phases (a) and (c).

$$(2.17) \quad \sigma^i = \begin{cases} 0 & \text{for } \varepsilon^i \leq (1 - \beta^i); \\ \sigma^{(a,i)} = k_0^i (\varepsilon_i - (1 - \beta^i)) / (1 - \varepsilon^i) & \text{for } ((1 - \beta^i) < \varepsilon^i < \bar{\varepsilon}_a^i) \text{ or} \\ & ((\bar{\varepsilon}_a^i < \varepsilon^i < \varepsilon_\beta^i) \text{ and } (\text{flag}^{(k-1)} \neq c)); \\ \sigma^{(c,i)} = k_c^i (\varepsilon^i - (1 - \beta^i) - \beta^i \varepsilon_*^i) / (1 - (\varepsilon^i - \beta^i \varepsilon_*^i)) & \text{for } (\varepsilon^i > \varepsilon_c^i) \text{ or} \\ & ((\bar{\varepsilon}_c^i < \varepsilon^i < \varepsilon_c^i) \text{ and } (\text{flag}^{(k-1)} \neq a)); \\ \sigma^{(d,i)} = \sigma_a^i + k_{p+}^i (\varepsilon^i - \varepsilon_a^i) & \text{for } (\varepsilon_a^i \leq \varepsilon^i \leq \varepsilon_c^i) \text{ and } (\text{flag}^{(k-1)} = a); \\ \sigma^{(e,i)} = \bar{\sigma}_c^i + k_{p-}^i (\varepsilon^i - \bar{\varepsilon}_c^i) & \text{for } (\bar{\varepsilon}_a^i \leq \varepsilon^i \leq \bar{\varepsilon}_c^i) \text{ and } (\text{flag}^{(k-1)} = c); \end{cases}$$

where, at the generic step k of a quasistatic loading process, it results that

$$\text{flag}^{(k)} = a \text{ if } \sigma^i = \sigma^{(a,i)}; \quad \text{flag}^{(k)} = c \text{ if } \sigma^i = \sigma^{(c,i)}; \quad \text{flag}^{(k)} = \text{flag}^{(k-1)} \text{ otherwise.}$$

The stress-strain equation (2.17) can be characterized in terms of the independent parameters β^i , k_0^i , k_c^i , k_{p+}^i , k_{p-}^i , ε_a^i , ε_c^i , and $\Delta\sigma^i = \sigma_a^i - \bar{\sigma}_c^i$. The quantities k_0^i and k_c^i represent the slopes of the branches (a) and (c) at zero stress, respectively (Figure 6). The quantities k_{p+}^i and k_{p-}^i instead denote the slopes of the “plastic” transition branches (d) and (e), respectively. As already discussed, we allow for nonzero stiffness of such branches in order to account for graded mechanical properties of the foam at the microscopic scale. Let (a') denote the particularization of branch (a) for $\beta^i = 1$ (Figure 6), and set $\sigma^{(a',i)} = k_0^i \varepsilon^i / (1 - \varepsilon^i)$. The parameters ε_a^i and ε_c^i represent the transition strains from phase (a') to phase (d) and from phase (d) to

phase (c), respectively. Finally, $\beta^i \in (0, 1]$ represents the integrity parameter of the current spring; the quantity $1 - \beta^i \in [0, 1)$ denotes the activation strain (or damage parameter), while $\Delta\sigma^i$ represents the stress drop moving from point A to point C (Figure 6).

The remaining quantities appearing in (2.17) can easily be derived from the above independent parameters. In particular, one computes ε_β^i , ε_*^i , $\bar{\varepsilon}_c^i$ and $\bar{\varepsilon}_a^i$ by solving the equations

$$\begin{aligned}\sigma^{(a,i)}(\varepsilon^i = \varepsilon_\beta^i) &= \sigma^{(d,i)}(\varepsilon^i = \varepsilon_\beta^i), \\ \sigma^{(b,i)}(\varepsilon^i = \varepsilon_a^i) &= \sigma^{(c,i)}(\varepsilon^i = \varepsilon_a^i), \\ \sigma^{(c,i)}(\varepsilon^i = \bar{\varepsilon}_c^i) &= \sigma^{(e,i)}(\varepsilon^i = \bar{\varepsilon}_c^i), \\ \sigma^{(e,i)}(\varepsilon^i = \bar{\varepsilon}_a^i) &= \sigma^{(a,i)}(\varepsilon^i = \bar{\varepsilon}_a^i)\end{aligned}$$

for such variables, respectively. It is seen from Figure 6 that the “damaged” stress-strain response ($\beta < 1$) returns to the primary loading path (a’)-(d) for $\varepsilon \geq \varepsilon_\beta^i$.

From now on, we use the symbol N to denote the number of mesoscopic springs that form the macroscopic mass-spring model. At a given loading step k (that is, for a given prescribed displacement \bar{u}_k of the topmost mass), we compute the corresponding (macroscopic) equilibrium configuration of the system through a dynamical relaxation procedure. The latter is founded upon the integration with respect to a virtual (or “internal”) time t of the equations of motion

$$(2.18) \quad m^i \ddot{u}_N^i + \gamma^i \dot{u}_N^i = \sigma^{i+1} - \sigma^i, \quad i = 1, \dots, N,$$

under the initial boundary conditions

$$(2.19) \quad \begin{aligned}\hat{u}_N^i(t=0) &= (u_N^i)^{(k-1)}, \quad i = 0, \dots, N-1; \quad \hat{u}_N^N(t=0) = \bar{u}_k; \\ \hat{u}_N^i(t=0) &= 0, \quad i = 0, \dots, N.\end{aligned}$$

Here, $\hat{u}_N^i = \hat{u}_N^i(t)$ denote transient displacement histories of the masses m^0, \dots, m^N forming the macroscopic model; a superimposed dot denotes a derivative with respect to t ; and $\gamma^1, \dots, \gamma^N$ denote the (“critical”) damping coefficients

$$\gamma^i = 2 \sqrt{m^i k^i},$$

where $k^i = d\sigma^i/d\varepsilon^i$ indicates the stiffness of the i th spring at the beginning of the current loading step. Equations (2.18) are numerically integrated through a fourth-order Runge–Kutta integration scheme, up to an internal time t_1 such that it results [14] in

$$|\sigma^{i+1} - \sigma^i| \leq 10^{-6} |\sigma^N| \quad \text{for all } i \in \{1, \dots, N-1\}.$$

3. Applications. We illustrate the macroscopic model formulated in the previous section by applying it to the simulation of the cyclic compression experiment illustrated in Figure 1. Such an experiment was performed on a single-layer CNT array with 0.847 mm thickness, which was synthesized using a vapor phase (or “floating catalyst”) thermal chemical vapor deposition (CVD) system, as described elsewhere [1, 31]. Following past work, the composition of the flow gas used during synthesis has a large effect on the resulting structure and mechanical response of the CNT arrays

[31]. An inert gas such as argon is typically used during CVD synthesis of CNTs, with a reducing agent such as hydrogen sometimes included to prevent impurities. It has been observed that increasing the H₂/Ar ratio can result in CNTs of narrower diameters and CNT arrays with a much more compliant response [31]. The compression test in Figure 1 was performed on a sample synthesized in 50% Ar, 50% H₂, with CNTs of diameter ~ 18 nm. The compression tests were performed quasistatically at strain rates of $\dot{\epsilon} = 0.03s^{-1}$ using a commercial materials testing system (Instron E3000). The sample was compressed three times to a maximum overall strain of $\epsilon = 0.4$ and then three times to a maximum strain of $\epsilon = 0.8$.

We focus our attention on the first loading-unloading path to $\epsilon = 0.4$ (1st cycle to 0.4 in Figure 1, hereafter also denoted as *np*), and the first loading-unloading path to $\epsilon = 0.8$, which follows preconditioning at $\epsilon = 0.4$ (1st cycle to 0.8 in Figure 1, hereafter also denoted as *wp*). We fit the mechanical properties of single-spring and multispring models to the experimental stress-strain curves, making use of the Genetic Algorithm procedure illustrated in [14] and the normalized root-mean-square deviation (NRMSD)

$$(3.1) \quad f = \frac{\sqrt{\frac{\sum_{k=1}^{N_{\text{data}}} (\sigma_k^{\text{mod}} - \sigma_k^{\text{exp}})^2}{N_{\text{data}}}}}{(\sigma_{\text{max}}^{\text{exp}} - \sigma_{\text{min}}^{\text{exp}})}$$

as fitting performance. In (3.1), N_{data} denotes the number of experimental data points, σ_k^{exp} the experimental value of the stress in correspondence with the loading step $\epsilon = \epsilon_k$, and σ_k^{mod} denotes the predicted stress for $\epsilon = \epsilon_k$.

In Figures 7 and 8, comparisons between experimental and best-fit overall stress-strain curves are shown, while the best-fit values of the mechanical properties of the fitting models are provided in Tables 1 and 2, together with the corresponding fitting performances.

We obtain rather good fitting performances already through single-spring models (NRMSD equal to 4.3% and 4.8% for the cases *np* and *wp*, respectively). In such a case, the behavior after preconditioning (*wp*-model) corresponds to $\beta = 0.83$ (Table 1), which implies an activation strain $\epsilon = 0.17$ (Figure 7). Snapshots of the deformation history of the single-spring *np* and *wp* models are illustrated in Figure 9. One can easily recognize that the first loaded ($\sigma > 0$) equilibrium configuration of the *wp* model (first configuration in Figure 7, *wp*) features total height $h_{\text{wp}} = 0.83h_{\text{np}}$, where h_{np} denotes the undeformed height of the *np* model.

Appreciable improvements of the fitting performance are observed in the five spring models, which indeed shows NRMSD equal to 3.2% and 4.4% in the *np* and *wp* cases, respectively (cf. Figure 8 and Table 2). The fitting algorithm adopted for such a model includes a grading-constraint which requires that the springs placed at the bottom of the chain collapse before than those placed at the top (we number the springs progressively from bottom to top, cf. section 2.1). This choice is based on the physical gradients that are known to exist in these materials (see below). It is worth noting that the examined models feature uniform stiffness parameters $k_0 = 4.27$ MPa and $k_c = 15.7k_0$ in each spring (Table 2). The results shown in Table 2 and Figure 10 highlight that the five spring model localizes in the bottommost spring (#1-*wp*) all the preconditioning damage corresponding to the *wp* case. Such a spring exhibits a local activation strain $\epsilon^1 = 0.90$ (the corresponding integrity parameter β^1 is indeed equal to 0.10; cf. Table 2), while the overall activation strain is approximately equal to 0.17 (Figure 8). The bottom-top collapse mechanisms of the five spring models (Figure 10)

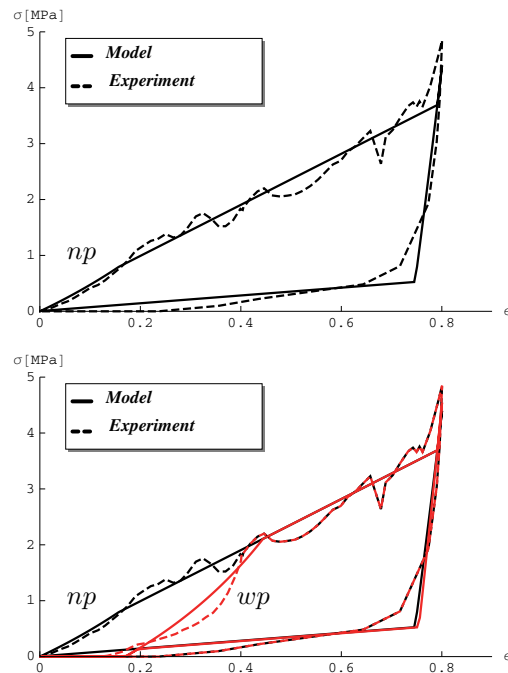


FIG. 7. Fitting of the experimental response illustrated in Figure 1 to single-spring models, without preconditioning (np : black curves), and with preconditioning at $\varepsilon = 0.4$ (wp : red curves). (Color available online.) Spring properties in Table 1.

follow from the increasing values of the transition strains ε_a^i of the different springs (Table 2). In particular, Figure 10, np shows that the five spring np model features sequential collapse of the springs #1, #2, #3, and #4 (Figure 10, np). The topmost spring #5- np instead jumps from phase (a) to phase (c) without collapsing (cf. Table 2 and Figure 10, np). On the other hand, the five spring wp model first features the complete collapse of the predamaged spring #1 (configuration #2 in Figure 10, wp) and then the sequential collapse of springs #2, #3, and #4 (cf. configurations #3 to #5 in Figure 10, wp). As in the np case, spring #5 jumps from phase (a) to phase (c) without collapsing (Table 2 and Figure 10, wp).

This matches previous work with real CNT foams in which the same sequential buckling from the base upward is observed. Clear images of this phenomenon can be observed in the work [18], closely matched by the configuration of springs seen in Figure 10. Physically, this strain localization arises due to known gradients in certain physical properties along the height of the structures, such as in density [29] and CNT diameter [20]. Because of the lateral interactions of CNTs, this localized strain is accommodated by the formation of buckles, which result from the reorientation and collective buckling of CNTs [37]. Additionally, these physical gradients are sufficiently large—and therefore the mechanical properties vary significantly as a function of height—that while a buckle is in the process of forming at the base of the structure, the rest of the structure remains undeformed. Thus the strain localization observed in Figure 10 is in agreement with experimental observations.

4. Concluding remarks. We have shown in this paper that a bistable-mass-spring model is able to incorporate the effect of damage in the hysteretic response

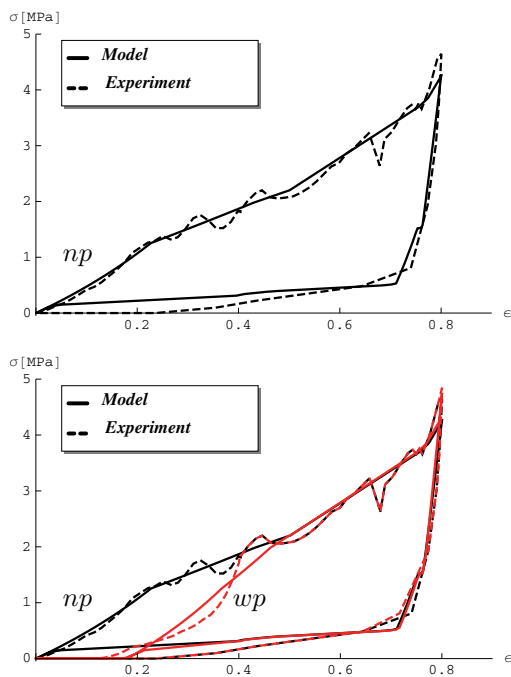


FIG. 8. Fitting of the experimental response illustrated in Figure 1 to five spring models, without preconditioning (*np*: black curves), and with preconditioning at $\epsilon = 0.4$ (*wp*: red curves). (Color available online.) Spring properties in Table 2.

TABLE 1

Mechanical properties of single-spring models fitting results in Figure 1, without preconditioning (*np*), and with preconditioning at $\epsilon = 0.4$ (*wp*).

Spring #	β	k_0 [MPa]	$\Delta\sigma/\sigma_a$	ϵ_a	ϵ_c	k_{p+}/k_0	k_{p-}/k_0	k_c/k_0	f
1 - <i>np</i>	1.000	4.270	-0.338	0.157	0.791	1.069	0.159	15.700	0.043
1 - <i>wp</i>	0.830	4.270	-0.338	0.157	0.791	1.069	0.159	15.700	0.048

TABLE 2

Mechanical properties of five spring models fitting results in Figure 1, without preconditioning (*np*), and with preconditioning at $\epsilon = 0.4$ (*wp*).

Spring #	β	k_0 [MPa]	$\Delta\sigma/\sigma_a$	ϵ_a	ϵ_c	k_{p+}/k_0	k_{p-}/k_0	k_c/k_0	f
5 - <i>np</i>	1.000	4.270	-0.228	0.317	0.317	0.851	0.046	15.700	
4 - <i>np</i>	1.000	4.270	-0.737	0.317	0.788	0.851	0.046	15.700	
3 - <i>np</i>	1.000	4.270	-0.749	0.317	0.939	0.851	0.046	15.700	
2 - <i>np</i>	1.000	4.270	-0.749	0.227	0.942	0.851	0.046	15.700	
1 - <i>np</i>	1.000	4.270	-0.749	0.227	0.942	0.310	0.046	15.700	0.031
5 - <i>wp</i>	1.000	4.270	-0.228	0.317	0.317	0.851	0.046	15.700	
4 - <i>wp</i>	1.000	4.270	-0.737	0.317	0.788	0.851	0.046	15.700	
3 - <i>wp</i>	1.000	4.270	-0.749	0.317	0.939	0.851	0.046	15.700	
2 - <i>wp</i>	1.000	4.270	-0.749	0.227	0.941	0.851	0.046	15.700	
1 - <i>wp</i>	0.100	4.270	-0.749	0.227	0.941	0.310	0.046	15.700	0.044

of a CNT array. With respect to the model recently presented in [14], we have allowed for the possible failure of material bondings, represented by the weakening of certain springs in the one-dimensional network. We have demonstrated that such a

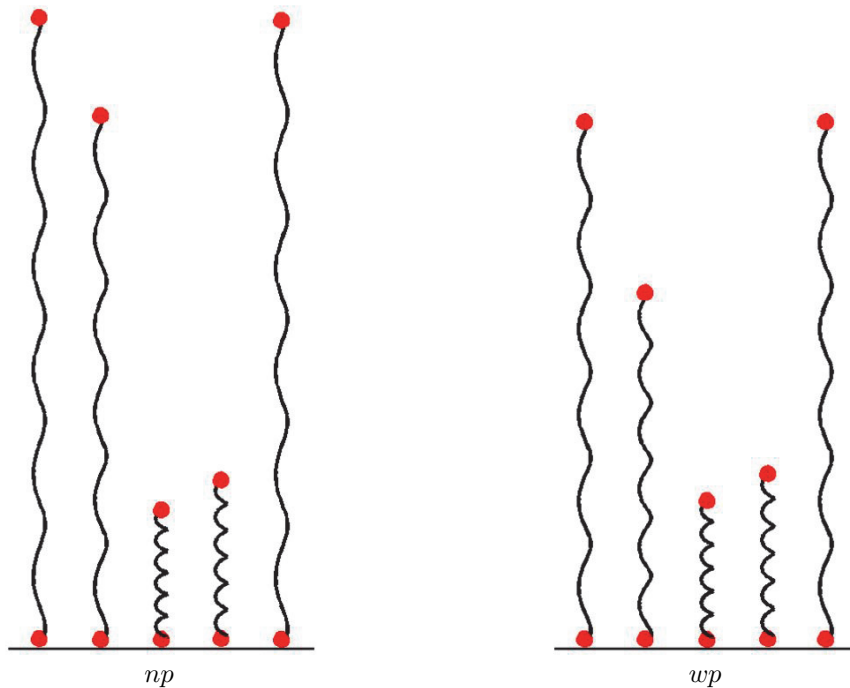


FIG. 9. Snapshots of the deformation histories of the single-spring models. Spring properties in Table 1.

generalization of the model presented in [14] is capable of handling preconditioning-induced material damage, characterized by a nonzero activation strain; permanent deformation; and a progressive reduction in the energy dissipation capacity of the system. The change in the permanent deformation goes along with a change of the activation strain. As one main benefit, we are now in the position to extend the concept of “transformational plasticity” given in [28] from time-independent hysteretic behavior to fatigue-type material damage. This opens a large class of new applications, in particular the materials with Mullins-like behavior [23] that include, beside carbon nanotube arrays, rubber-like and soft biological materials.

The bistable spring model presented here is an interesting generalization of the fundamental mechanism developed in [28]. In contrast to the theory presented therein, due to considering nonlinear kinematics, we can derive a stress-strain law of the stable branches (a) and (c) permitting us to have in the limit $\delta \searrow 0$ springs with zero stiffness bearing nonzero stresses. The internal damage parameter is related to the number of hysteretic shakedowns applied to the material during the previous loading history (up to different maximum strains). As a result, we obtain a fatigue-type damage model that is rate-independent and contemplates the return of the material to the primary loading path for a suitable value of the overall strain, which is suitably larger than the activation strain.

The present work represents a first step towards the formulation of a unified damage model of CNT arrays, which includes the formulation of a suitable evolution law of β . The latter might be formulated, e.g., on the basis of the pseudoelastic

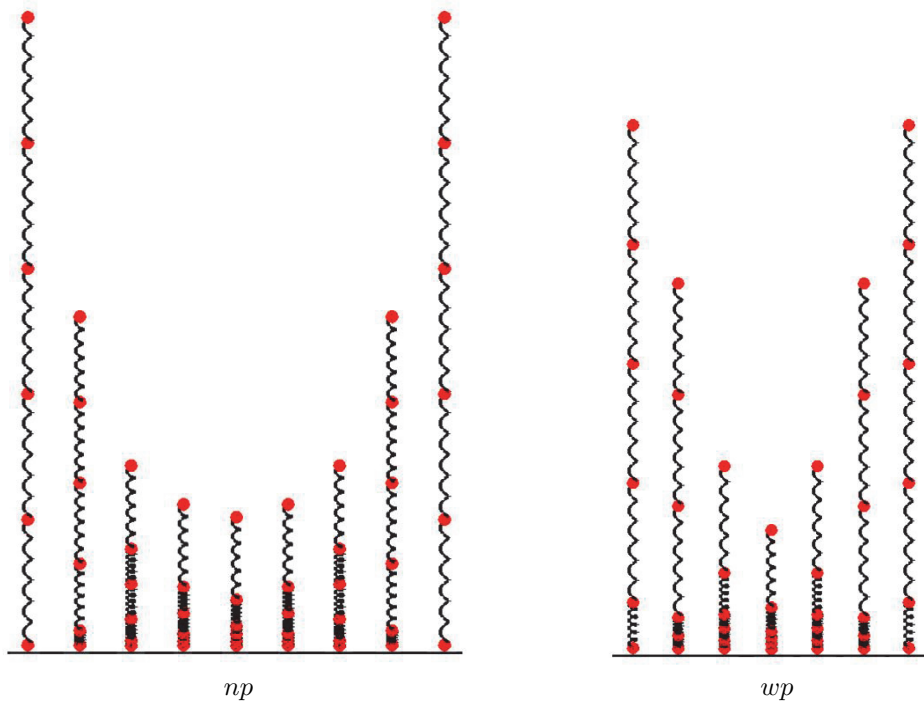


FIG. 10. Snapshots of the deformation histories of the five spring models. Spring properties in Table 2.

approach given in [9], or the generalized damage model presented in [19].

The macroscopic model formulated in section 2.3 allowed us to generalize the analytic mesoscopic model developed in section 2.2, in order to account for graded material properties along the height of the CNT array [29, 18]. The numerical simulation of a compression experiment on a real CNT foam has shown that such a model is actually able to capture the experimental macroscopic stress-strain behavior, before and after preconditioning; damage localization at the basis of the structure; and sequential buckling from the base upward. The latter phenomena are well recognized in the literature dealing with the experimental behavior of CNT foams [29, 20, 37, 18].

We leave to future work the modeling of the transient mechanical response of CNT structures during preconditioning, accounting for progressive deterioration of the material stiffness at different scales, as well as the formulation and the experimental validation of the evolution law of the integrity parameter β . Future research lines also include an analytic study on the limiting dissipative behavior of bistable spring chains featuring nonuniform material properties; the modeling of the mechanical response of multilayer CNT structures; and the in situ identification of material properties, to be carried out through high-resolution camera- and/or SEM-assisted laboratory tests, [18, 30, 15].

Acknowledgments. The authors gratefully acknowledge the support received from Ada Amendola (Department of Civil Engineering, University of Salerno) during the course of the present work.

REFERENCES

- [1] R. ANDREWS, D. JACQUES, A. M. RAO, F. DERBYSHIRE, D. QIAN, X. FAN, E. C. DICKEY, AND J. CHEN, *Continuous production of aligned carbon nanotubes: A step closer to commercial realization*, Chem. Phys. Lett., 303 (1999), pp. 467–474.
- [2] R. H. BAUGHMAN, A. A. ZAKHIDOV, AND W. A. DE HEER, *Carbon nanotubes—the route toward applications*, Science, 297 (2002), pp. 787–792.
- [3] G. BERTOTTI, *Energetic and thermodynamic aspects of hysteresis*, Phys. Rev. Lett., 76 (1996), pp. 1739–1742.
- [4] T. BLESSEN, F. FRATERNALI, J. R. RANEY, A. AMENDOLA, AND C. DARAIO, *Continuum limits of bistable spring models of carbon nanotube arrays accounting for material damage*, Mech. Res. Commun., 45 (2012), pp. 58–63.
- [5] P. D. BRADFORD, X. WANG, H. ZHAO, AND Y. ZHU, *Tuning the compressive mechanical properties of carbon nanotube foam*, Carbon, 48 (2011), pp. 2834–2841.
- [6] A. CAO, P. DICKRELL, W. G. SAWYER, M. GHASEMI-NEIHAD, AND P. AJAYAN, *Supercompressible foamlike carbon nanotube films*, Science, 310 (2005), pp. 1307–1310.
- [7] D. DE TOMMASI AND G. PUGLISI, *A micromechanics-based model for the Mullins effect*, J. Rheol., 50 (2006), pp. 495–512.
- [8] D. DE TOMMASI, G. PUGLISI, AND G. SACCOMANDI, *Damage, self-healing, and hysteresis in spider silks*, Biophys. J., 98 (2010), pp. 1941–1948.
- [9] A. DORFMANN AND R. W. OGDEN, *A constitutive model for the Mullins effect with permanent set in particle-reinforced rubber*, Int. J. Solids Struct., 41 (2004), pp. 1855–1878.
- [10] M. R. FALVO, G. J. CLARY, R. M. TAYLOR, V. CHI, F. P. BROOKS, S. WASHBURN, AND R. SUPERFINE, *Bending and buckling of carbon nanotubes under large strain*, Nature, 389 (1997), pp. 582–584.
- [11] D. S. FISHER, *Collective transport in random media: From superconductors to earthquakes*, Phys. Rep., 301 (1998), pp. 113–150.
- [12] M. FLAMM, J. SPRECKELS, T. STEINWEGER, AND U. WELTIN, *Effects of very high loads on fatigue life of NR elastomer materials*, Int. J. Fatigue, 33 (2011), pp. 1189–1198.
- [13] N. FORCADEL, C. IMBERT, AND R. MONNEAU, *Homogenization of some particle systems with two-body interactions and of the dislocation dynamics*, Discrete Contin. Dyn. Syst., 23 (2009), pp. 785–826.
- [14] F. FRATERNALI, T. BLESSEN, A. AMENDOLA, AND C. DARAIO, *Multiscale mass-spring models of carbon nanotube foams*, J. Mech. Phys. Solids, 59 (2011), pp. 89–102.
- [15] F. FRATERNALI, J. R. RANEY, AND C. DARAIO, *Modeling microscale instabilities in compressed carbon nanotube bundles using multistable spring models*, Compos. Struct., 96 (2013), pp. 745–750.
- [16] L. J. GIBSON AND M. F. ASHBY, *Cellular Solids: Structure and Property*, 2nd ed., Pergamon Press, Oxford, UK, 1999.
- [17] Y. J. HE AND Q. P. SUN, *Rate-dependent domain spacing in a stretched NiTi strip*, Int. J. Solids Struct., 47 (2010), pp. 2775–2783.
- [18] S. B. HUTCHENS, L. HALL, AND J. R. GREER, *In situ mechanical testing reveals periodic buckle nucleation and propagation in carbon nanotube bundles*, Adv. Funct. Mater., 20 (2010), pp. 1–9.
- [19] J. LEMAITRE AND R. DESMORAT, *Engineering Damage Mechanics: Ductile, Creep, Fatigue and Brittle Failures*, Springer, Berlin, 2005.
- [20] X. S. LI, X. F. ZHANG, L. J. CI, R. SHAH, C. WOLFE, S. KAR, S. TALAPATRA, AND P. M. AJAYAN, *Air-assisted growth of ultra-long carbon nanotube bundles*, Nanotechnology, 19 (2008), 455609.
- [21] A. MISRA, J. R. GREER, AND C. DARAIO, *Strain rate effects in the mechanical response of polymer anchored carbon nanotube foams*, Adv. Mater., 21 (2009), pp. 334–338.
- [22] A. MISRA, J. R. RANEY, L. DE NARDO, A. CRAIG, AND C. DARAIO, *Synthesis and characterization of carbon nanotube polymer multilayer structures*, ACS Nano, 5 (2011), pp. 7713–7721.
- [23] L. MULLINS, *Effect of stretching on the properties of rubber*, J. Rubber Res., 16 (1947), pp. 275–289.
- [24] G. PAMPOLINI AND G. DEL PIERO, *Strain localization in open-cell polyurethane foams: Experiments and theoretical model*, J. Mech. Mater. Struct., 3 (2008), pp. 969–981.
- [25] E. PEÑA, *Prediction of the softening and damage effects with permanent set in fibrous biological materials*, J. Mech. Phys. Solids, 59 (2011), pp. 1808–1822.
- [26] H. PETRYK AND S. STUPKIEWICZ, *Interfacial energy and dissipation in martensitic phase transformations. Part I: Theory*, J. Mech. Phys. Solids, 58 (2010), pp. 390–408.
- [27] G. PUGLISI AND L. TRUSKINOVSKY, *Rate independent hysteresis in a bi-stable chain*, J. Mech. Phys. Solids, 50 (2002), pp. 165–187.

- [28] G. PUGLISI AND L. TRUSKINOVSKY, *Thermodynamics of rate-independent plasticity*, J. Mech. Phys. Solids, 53 (2005), pp. 655–679.
- [29] V. L. PUSHPARAJ, L. CI, S. SREEKALA, A. KUMAR, S. KESAPRAGADA, D. GALL, O. NALAMASU, A. M. PULICKEL, AND J. SUHR, *Effects of compressive strains on electrical conductivities of a macroscale carbon nanotube block*, Appl. Phys. Lett., 91 (2007), 153116.
- [30] J. R. RANEY, F. FRATERNALI, A. AMENDOLA, AND C. DARAIO, *Modeling and in situ identification of material parameters for layered structures based on carbon nanotube arrays*, Compos. Struct., 93 (2011), pp. 3013–3018.
- [31] J. R. RANEY, A. MISRA, AND C. DARAIO, *Tailoring the microstructure and mechanical properties of arrays of aligned multiwall carbon nanotubes by utilizing different hydrogen concentrations during synthesis*, Carbon, 49 (2011), pp. 3631–3638.
- [32] J. SUHR, P. VICTOR, L. CI, S. SREEKALA, X. ZHANG, O. NALAMASU, AND P. AJAYAN, *Fatigue resistance of aligned carbon nanotube arrays under cyclic compression*, Nat. Nanotechnol., 2 (2007), pp. 417–421.
- [33] O. YAGLIOGLU, *Carbon Nanotube Based Electromechanical Probes*, Ph.D. thesis, Massachusetts Institute of Technology, Cambridge, MA, 2007.
- [34] X. YANG, P. HE, AND H. GAO, *Modeling frequency- and temperature-invariant dissipative behaviors of randomly entangled carbon nanotube networks under cyclic loading*, Nano Res., 4 (2011), pp. 1191–1198.
- [35] H. YAP, R. LAKES, AND R. CARPICK, *Mechanical instabilities of individual multiwalled carbon nanotubes under cyclic axial compression*, Nano Lett., 7 (2007), pp. 1149–1154.
- [36] H. YAP, R. LAKES, AND R. CARPICK, *Negative stiffness and enhanced damping of individual multiwalled carbon nanotubes*, Phys. Rev. B, 77 (2008), 045423.
- [37] A. A. ZBIB, S. DJ. MESAROVIC, E. T. LILLEODDEN, D. MCCLAIN, J. JIAO, AND D. F. BAHR, *The coordinated buckling of carbon nanotube turfs under uniform compression*, Nanotechnology, 19 (2008), 175704.